Bull Mater Sci (2020)43:224
https://doi.org/10.1007/s12034-020-02198-0

Design and synthesis of organic dyes with various donor groups: promising dyes for dye-sensitized solar cells

ABDULLAH G AL-SEHEMI[1,2], SHUHRAH ALI S ALLAMI[1] and ABUL KALAM[1,2,*]

[1]Department of Chemistry, Faculty of Science, King Khalid University, Abha 61413, Saudi Arabia
[2]Research Center for Advanced Materials Science (RCAMS), King Khalid University, Abha 61413, Saudi Arabia
*Author for correspondence (abul_k33@yahoo.com)

MS received 23 January 2020; accepted 12 March 2020

Abstract. The present work is involved in the computational and experimental studies of organic dyes and their applications as dye-sensitized solar cells (DSSCs). This comprised the study of three hydrazone-based sensitizers (*E*)-2-cyano-*N*′-((2-hydroxynaphthalen-1-yl)methylene)acetohydrazide (CHMA), (*E*)-2-cyano-*N*′-(4-(dimethylamino)benzylidene)acetohydrazide (CDBA), (*E*)-*N*′-(anthracen-9-ylmethylene)-2-cyanoacetohydrazide (AMCH) that have been prepared and confirmed by means of several analytical procedures like Fourier transform infrared, UV–visible and nuclear magnetic resonance techniques to investigate the best possible selection for DSSCs by computational and experimental techniques. The computational methods are applied to optimize the structures of prepared organic dyes *via* density functional theory (DFT) method at B3LYP/6-311G(p,d) level of theory. The time-dependent DFT (TD-B3LYP/6-311G**) was used with and without solvent to find out the absorption spectra and matched with the experimental data and the electro-optical and reorganization energies of prepared dyes were further investigated. The results revealed that the prepared dyes would be better sensitizers for DSSCs because of small highest-occupied molecular orbital–lowest-unoccupied molecular orbital energy gap. Moreover, on the basis of the above results, we fabricated the devices *via* the doctor blade method to study the photovoltaic performance with the prepared dyes (CHMA, CDBA and AMCH). The dye AMCH exhibited the maximum efficiency with commercial TiO_2.

Keywords. Dye-sensitized solar cell; efficiency; density functional theory; electronic properties; time-dependent density functional theory.

1. Introduction

The conservative assets like fossil fuels are the main source for energy and the whole world depends on these sources. These sources are not eco-friendly, non-renewable, release carbon dioxide gas and by time will reduce. The solar energy, hydro energy and wind energy are the main source of renewable energy which is eco-friendly and economical. Among them, solar energy is freely available, clean and environment-friendly and utmost encouraging as an upcoming renewable energy source. The energy intake is estimated at approximately 28 TW by 2050 [1]. In photovoltaics, dye-sensitized solar cells (DSSCs) create extensive curiosity for renewable energy due to its environment-friendly benefits, low manufacturing costs and huge scale growth [2–5] as compared to Si-based devices [6,7]. Since 1991, different kinds of photosensitizers like ruthenium-based dyes, organic dyes and porphyrin dyes have been prepared to develop extremely competent and stable DSSCs [8–11]. But the organic dyes have attracted more attention of researchers due to eco-friendliness, low cost and easy to production [12,13]. The main problem with the organic solar cell is its low efficiency and stability of the devices [14]. Varieties of organic and natural dyes have been studied and used in DSSCs as low-cost sensitizers last year [15–22]. The natural pigments, such as annatto pigments derived from *Bixa orellana* seeds, achieved conversion efficiencies up to around 0.53% in dye-sensitized titanium dioxide (TiO_2) solar cells [23]. The natural pigments obtained from rosella and blue pea flowers and a medley of the extracts achieved efficiencies 0.37, 0.05 and 0.15%, respectively [24]. A major target in this field is an improvement of the conversion efficiency by structural modification, so the donor (D) and acceptor (A) systems separated by a π-conjugated bridge become a new trend in dye design [22]. Several donor groups, such as heteroanthracene, anthraquinone, indoline, tetrahydroquinoline, boradiazaindacene,

Electronic supplementary material: The online version of this article (https://doi.org/10.1007/s12034-020-02198-0) contains supplementary material, which is available to authorized users.

Published online: 20 August 2020

carbazole, merocyanine, squaraine, triarylamine and cyanoacrylic acid, etc., have been examined [7]. Metal-free organic dyes on TiO_2 semiconductors have shown the highest efficiencies. Two metal-free organic sensitizers with thienothiophene and theophany substitutes have reported high efficiency up to 6.23% [25]. New organic dyes containing moieties of *N*,*N*-dimethylaniline as donors and a moiety of cyanoacetic acid as acceptor have achieved an efficiency up to 6.8% with $J_{sc} = 12.9$ mA cm^{-2}, $V_{oc} = 0.71$ V under AM 1.5 irradiation (100 mW cm^{-2}) [26]. Hydrazone derivatives were widely known due to their desirable characteristics such as lower cost, easy synthesis and characterization, ability to quickly charge-transport [27] and reaction with nucleophilic and electrophilic reagents [28]. Hydrazones have been skillfully employed in numerous applications, including metal–organic frameworks [29], dynamic combinatorial chemistry [30], hole transport materials (HTMs) [27] and dyes [31]. Thiophene-based hydrazones were synthesized involving reactive vinyl groups and the optical, thermal and photoelectrical properties were examined and the hole-drift mobility at the high applied electric field was 10^{-5} cm^2 V^{-1} s^{-1} [32]. A sequence of the thiophene-based glass-forming hole-transporting hydrazones was designed and prepared and the optical, thermal and photoelectrical characteristics were characterized. The drift mobilities for the hole were 10^{-6} cm^2 V^{-1} s^{-1} at an applied electric field of 6.4×10^{-5} V cm^{-1} [33]. Four novels of donor–π–acceptor (D–π–A) hydrazone sensitizers (HB, HP, HF and HT) including an *N*,*N*-diphenylhydrazone as donor unit with 2-cyanoacetic acid as an acceptor unit connected by a diverse aromatic bridge have been produced. The DSSC-based HP achieved high power conversion efficiencies (PCE) up to 7.74% ($J_{sc} = 16.17$ mA cm^{-2}, $V_{oc} = 0.69$ V, FF = 0.694) under AM 1.5 G (100 mW cm^{-2})-simulated solar irradiation [34,35]. The biscarbazole and terthiophene derivatives-based molecular glasses attached to hydrazone moieties 2CzMPH and 3TDPH as HTMs were designed, manufactured and applied in solid-state DSSCs [36]. The type of anchoring group, adsorption of dye on semiconductor and steric hindrance of the substituents perform a key role in the efficiency of testing solar cell devices [12,37–39].

The dyes that have donor–acceptor anchoring groups with an extended pi-conjugated structure fascinated the immense attention of the researchers. Therefore, in view of this work, we designed and synthesized three organic dyes ((*E*)-2-cyano-*N*′-((2-hydroxynaphthalen-1-yl)methylene) acetohydrazide (CHMA), (*E*)-2-cyano-*N*′-(4-(dimethylamino)benzylidene)acetohydrazide (CDBA) and (*E*)-*N*′-(anthracen-9-ylmethylene)-2-cyanoacetohydrazide (AMCH)) with different donor and acceptor groups in two steps with the aim to enhance the efficiency for DSSC applications. We discussed the structural and optoelectronic properties of all prepared organic dyes by using Fourier transform infrared spectroscopy (FT-IR), UV–visible spectroscopy, nuclear magnetic resonance (^{1}H and ^{13}C NMR), density functional theory (DFT) and time-dependent DFT (TD-DFT) methods. The absorption band for organic dye (AMCH) was widened and red-shifted as compared to other two dyes (CHMA and CDBA). In addition, our aim is to understand the impact of donor and acceptor on the reorganization energies, electronic and optical properties.

2. Materials and methods

All chemicals are of analytical grade and used as received. Ethyl 2-cyanoacetate, hydrazine hydrate (80%), 4-dimethylaminobenzaldehyde, 2-hydroxy-1-naphthaldehyde, anthracene-9-carbaldehyde, acetic acid and ethanol were procured from Sigma-Aldrich. The reaction process was observed by TLC with the help of UV light. The commercial Ru sensitizer dye [di-tetrabutylammonium-*cis*-*bis*(isothiocyanato)*bis*(2,2′-bipyridyl-4,4′-dicarboxylato) ruthenium(II)] N719, electrolyte solution (Iodolyte AN-50, iodide/tri-iodide redox couple), platinum catalyst (T/SP paste), sealant (SX1170-60, 60 μm thick, DuPont Surlyn) and FTO-coated glass substrate (TCO 22-15, 2-mm thick glass with 15 Ω sq^{-1} surface resistivity) were obtained from Solaronix SA.

2.1 *Synthesis of 2-cyanoacetohydrazide*

A total of 2.21 g (44.1 mmol) hydrazine hydrate was slowly added to the solution of ethyl 2-cyanoacetate 5.0 g (44.1 mmol) in the ethanolic medium. The round-bottom flask was positioned in an ice bath with an amount of solid NaCl to decrease temperature to zero degrees under magnetic stirring. After 10 min of precipitation, the stirring was continued for complete precipitation at the same temperature. The white precipitate was filtered off, washed several times with ethanol and dried at room temperature. Yield: 96%; colour: off white; M.P.: 120–122°C; ^{1}H-NMR (500 MHz, DMSO) δ: 4.18 (2H, S), 5.9 (3H, S); ^{13}C-NMR (125 MHz, DMSO) δ: 173.0 (C-1, C=O), 38.2 (C-2, CH_2), 119.0 (C-3, C≡N); FT-IR (KBr) (cm^{-1}); 2255–3500, 2273, 1684, 1600 (scheme 1).

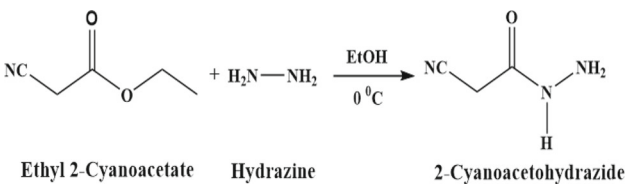

Scheme 1. Preparation scheme of 2-cyanoacetohydrazide.

2.2 *Synthesis of 2-cyano-N′-[(2-hydroxynaphthalen-1-yl)-methylene]acetohydrazide (CHMA)*

2-Hydroxy-1-naphthaldehyde 0.86 g (5 mmol) was dissolved in 20–30 ml of ethanol and added to the solution in 2-cyanoacetohydrazide 0.49 g (5 mmol). The round-bottom flask was attached to the reflux condenser with adjusting the heat at 100°C for 24 h. After that, one drop of acetic acid was added. The stirring was continued for complete precipitation at the same temperature, filtered off, washed with excess of ethanol and dried at room temperature. Yield: 87%, colour: yellow; M.P.: 162–166°C; ^{1}H-NMR (500 MHz, DMSO) δ: 4.2 (1H, s, CH); 3.9 (2H, s, CH_2); 10.67 (1H, s, NH); 11.7 (1H, s, OH); Ar-H: 8.75 (1H, d), 8.38 (1H, d), 7.94 (1H, m), 7.2 (1H, m), 7.5 (1H, d-d), 9.2 (1H, s); ^{13}C-NMR (125 MHz, DMSO) δ: 164.42 (C-1′, C=O), 24.17 (C-2′, CH_2), 121.0 (C-3′, C≡N), 151.05 (C-1″), 108.19 (C-1) M, 158.19 (C-2), 120.8 (C-3), 145.5 (C-4), 128.9 (C-5), 111.8 (C-6), 116.4 (C-7), 115.1 (C-8), 138.5 (C-9), 128.0 (C-10); FT-IR (KBr) (cm^{-1}); 3325 (NH), 3432 (OH), 2219 (C≡N), 1607 (C=N), 1665 (C=C), 1700 (C=O).

2.3 *Synthesis of 2-cyano-N′-[(4-dimethylamino)benzylidene]-acetohydrazide (CDBA)*

4-Dimethylamino benzaldehyde 0.29 g (2 mmol) solution was added to the solution in 2-cyanoacetohydrazide 0.19 g (2 mmol) and refluxed for 30 min at 100°C. Precipitation started after 30 min, the stirring was continued for complete precipitation at the same temperature, filtered off and washed with an excess of ethanol. Yield: 83%, colour: yellow; M.P.: 140–145°C; ^{1}H-NMR (500 MHz, DMSO) δ: 4.14 (1H, s, CH); 3.9 (2H, s, CH_2); 11.5 (1H, s, NH); Ar-H: [2H = 7.5 (d-d), 2H = 6.75 (d-d)]; 2.97 (6H, s, $(CH_3)_2$N); ^{13}C-NMR (125 MHz, DMSO) δ: 164.51 (C-1′, C=O), 24.19 (C-2′, CH_2), 121.1 (C-3′, C≡N), 148.11 (C-1″), 151.2 (C-1), 116.3 (C-2, 6), 129.4 (C-3, 5), 125.1 (C-4), 40.2 (–N $(CH_3)_2$); FT-IR (KBr) (cm^{-1}); 3325 (NH), 2815 (CH_3), 2219 (C≡N), 1607 (C=N), 1665 (C=C), 1700 (C=O).

2.4 *Synthesis of 2-cyano-N′-[(anthracen-9-yl)methylene]-acetohydrazide (AMCH)*

We followed the same procedure as mentioned previously, but instead of 4-dimethylamino benzaldehyde, 0.41 g (2 mmol) of anthracene-9-carbaldehyde solution was added to the solution in 2-cyanoacetohydrazide 0.19 g (2 mmol) and refluxed for 30 min at 100°C. Precipitation started after 30 min, the stirring was continued for complete precipitation at the same temperature, filtered off, washed with an excess of ethanol and dried at room temperature. Yield: 80%, colour: bright yellow; M.P.: 1443–148°C; ^{1}H-NMR (500 MHz, DMSO) δ: 4.2 (1H, s, CH); 3.9 (2H, s, CH_2); 9.22 (1H, s, NH); Ar-H: [2H = 7.6–7.68 (m, 2H; 8.6 (d, 4H); 8.2 (d, 4H); 8.76 (s, 1H)]; ^{13}C-NMR (125 MHz, DMSO) δ: 164.78 (C-1′, C=O), 24.96 (C-2′, CH_2), 121.3 (C-3′, C≡N), 143.5 (C-1″), 129.2 (C-1), 126.3 (C-2), 129.9 (C-9), 116.1 (C-10), 131.0 (C-10a); FT-IR (KBr) (cm^{-1}); 3325 (NH), 2219 (C≡N), 1607 (C=N), 1665 (C=C), 1700 (C=O) (scheme 2).

2.5 *Apparatus*

The melting points of the samples were obtained using the Stuart SMP30 melting point apparatus. The FT-IR spectra of prepared organic dyes were obtained by Shimadzu FT-IR 8400S infrared spectrophotometer using KBr pellets. The NMR (^{1}H and ^{13}C) spectra were obtained from a Bruker at 500 MHz and 125 MHz, respectively, Ultra Shield TM at room temperature in deuterated dimethyl sulphoxide (DMSO-d_6). The abbreviations are utilized s—singlet, d—doublet, m—multiplet. PG UV-160A spectrophotometer was used to record the UV–visible spectra in different solvents.

2.6 *Device fabrication*

The fluorine-coated tin oxide (FTO) glasses were cleaned in ethanol and acetone simultaneously for 20 min under ultrasonication. Additionally, by adopting the doctor blade method, TiO_2 and Pt pastes were spread on two different FTO glasses using a glass rod and dried in air to prepare the working electrode. The film was heated to 400°C for 30 min in the muffle furnace. The sensitization was carried out by immersing the working electrodes in the solution of prepared dyes (CHMA, CDBA and AMCH) for 24 h. After soaking the working electrode in the dye, these were washed in ethanol to remove excess dyes from the surface of the film.

2.7 *Assembling of cells*

The spacer from Meltonix was placed on the TiO_2 electrode such as a three-sided gasket, then a counter electrode was added facing down above the three-sided gasket and aligning with the stained dye region and one side is open for the injection of electrolyte. A suitable space at the edges of the two electrodes was left for contacts. The heat and pressure were measured on the electrodes. The electrolyte (Iodolyte HI30) filled into the fabricated cell through the capillary force from the open side. The open side of the cell was sealed with Araldite. The conductive material (silver paste) was then painted to obtain a good electrical flow. The copper wires were connected to the electrode. The positive terminal of the voltmeter was connected to the counter electrode (cathode), while the negative terminal of the voltmeter was connected to the TiO_2 layer electrode

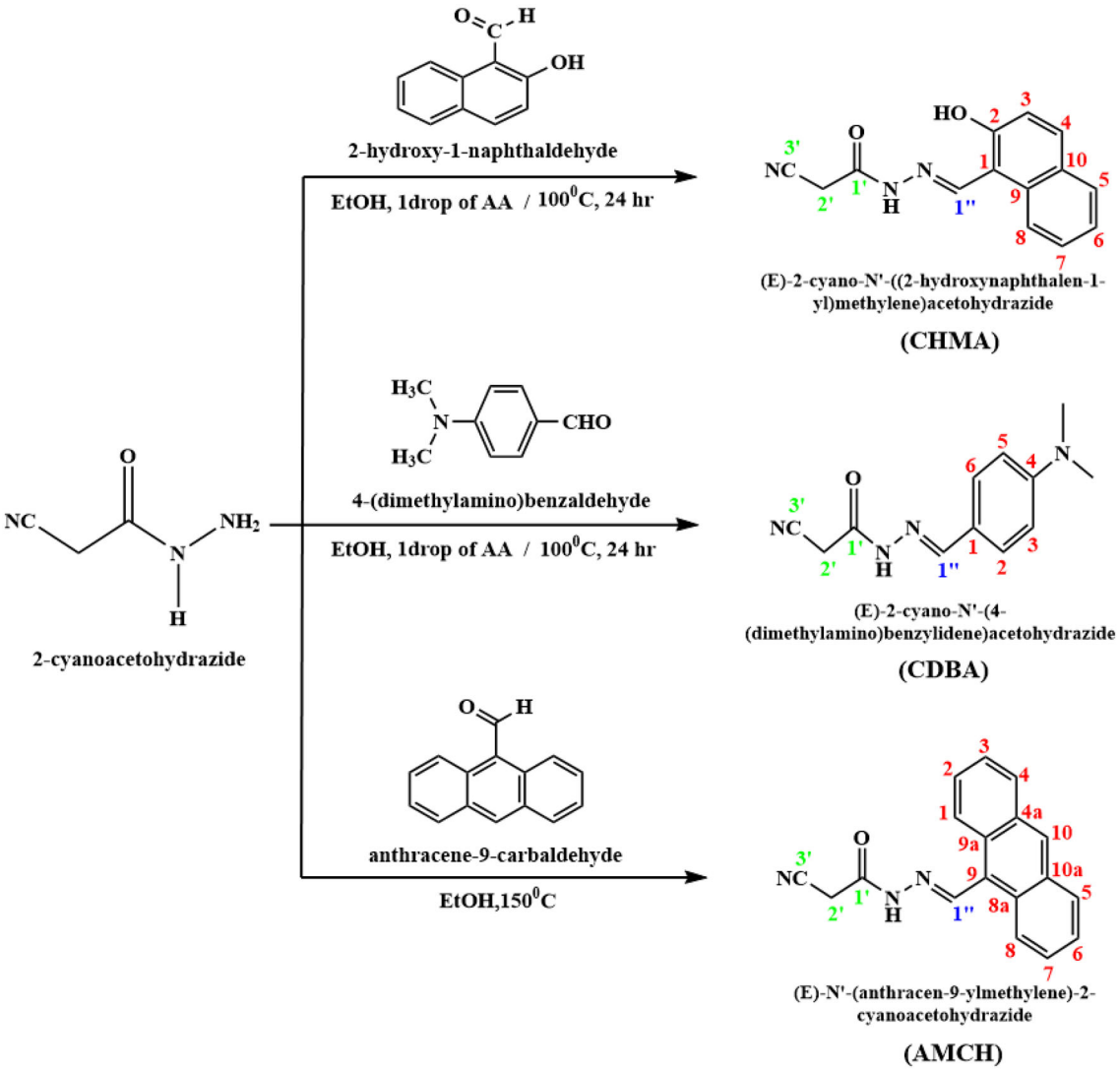

Scheme 2. Preparation schemes of dyes (CHMA, CDBA and AMCH).

(anode). The circuit voltage was measured under the solar cell current–voltage (*I–V*) characteristic measurement system.

2.8 *Computational details*

DFT has been extensively harnessed to figure the structural and chemical characteristics of classic inorganic and organic semiconductor materials [40]. DFT has been developed on the basis of the Hohenberg–Kohn theorem [41]. The geometry optimizations of the ground states have been carried out on the basis of the DFT [42]. TD-DFT has been employed as a prominent tool, in particular for studying the absorption spectra and structures of the sensitizers in DSSCs such as Ru complexes [43]. TD-DFT was also used for investigating several organic sensitizers [44]. DFT and TD-DFT have been trusted approaches for improving and clarifying the properties of electro-optical and charge transport (CT) and they are quite precise ways to get the experimental data back again [45]. As to the other methods of DFT, B3LYP approach introduces the most effective depiction of the modifications of the geometric on ionization [45]. B3LYP is an appropriate and harmonious function to study the value properties of the small or large organic pi (π)-conjugated molecules [46,47].

Recent studies specified that the B3LYP method was a better route to reproduce excitation energies for hydrazone-based dyes. Al-Sehemi *et al* [48] studies revealed that B3LYP the polarizable continuum model (PCM) method is superior, more precise and more sound route than BH and HLYP, LC-BLYP and CAM-B3LYP (the PCM method) to imitate the experimental data.

For the current study, we used the B3LYP method to compute the excitation energies and determined the solvent effects (DMSO, dimethylformamide (DMF), CH_3CN and C_2H_5OH) on the absorption spectra. Geometry optimizations for all dyes have been accomplished using DFT at the

B3LYP/6-311G(p,d) [49–53] level of theories. The energy gap and absorption spectra for prepared dyes were executed in different solvents (PCM) at TD-B3LYP/6-311G** level of theory [54–57]. The B3LYP/6-311G** level of theory has been applied to calculate the ionization potentials, electron affinities and reorganization energy (λ) of all dyes [58,59]. Gaussian-09 program package was used to accomplish the calculations [60].

3. Results and discussion

3.1 *Geometries*

The optimized geometrical parameters (bond lengths (Å), bond angles and dihedral angles (degrees)) of all three dyes have been listed in supplementary table S1 and complete optimized structures of CHMA and CDBA can be found in supplementary figures S1 and S2 of supporting information, whereas complete optimized structures of dye (AMCH) are presented in figure 1. We used the B3LYP/6-311G** level of theory for the optimization of the structure.

The impact of substituents on the geometries of selected bond length is shown in table 1. The C7–N8 of dye (CHMA) stretch 0.010 Å is compared to C10–N11 of dye (CDBA) and C7–N8 of dye (AMCH). The N11–N12 bond length in dye (CDBA) is almost similar to N8–N9 in dye (CHMA) and dye (AMCH), which are shortened 0.002 and 0.004 Å, respectively. In addition, bond length values of N12–C13 of dye (CDBA) and N9–C10 of dye (CHMA) lowered 0.010, and 0.001 Å respectively than N9–C10 in dye (AMCH). The calculated bond lengths of C10–O11 for both dye (CHMA) and dye (AMCH) are very well approximated with C13–O14, which lengthened 0.004 Å. Therefore, we can say that did not realize crucial changes from the substituents on the internuclear distances between the three prepared dyes.

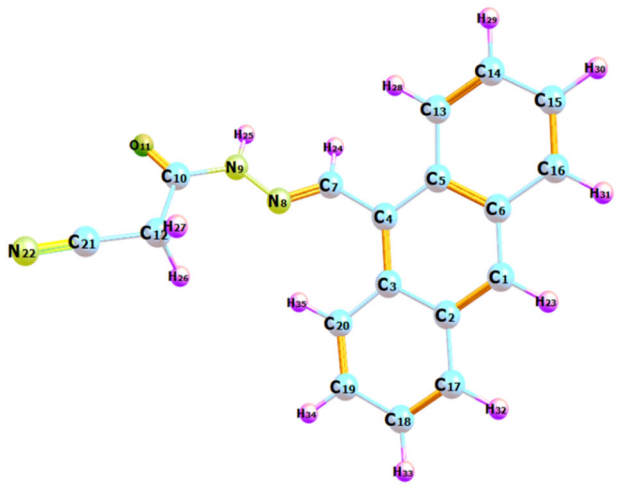

Figure 1. Optimized structure and atom numbering of dye (AMCH) in B3LYP/6-311G** level of theory.

3.2 *Electronic properties and absorption spectra*

Table 2 reports the computed highest-occupied molecular orbital energies (E_{HOMO}), lowest unoccupied molecular orbital energies (E_{LUMO}) and HOMO–LUMO energy gaps (E_{gap}) in the gas phase and different solvents. The calculated values for HOMO energies from B3LYP/6-311G** level of theory are −6.0 eV for dye (CHMA), −5.38 eV for dye (CDBA) and −5.71 eV for dye (AMCH), whereas LUMO energy values at the same level of theory are (−2.06 eV) for dye (CHMA), (−1.21 eV) for dye (CDBA) and (−2.76 eV) for dye (AMCH). The charge density in the HOMO that has π bonding character and LUMO that shows the character of a π* bonding orbital is delocalized over almost the entire molecule and the lone pair of electrons on the nitrogen atoms except for the nitrile group at the extremity of the molecules of the dyes (for dye (CHMA) and dye (CDBA) can be found in supplementary figures S3, S4 and figure 2). The HOMO energies (E_{HOMO}) would have been in the sequence of dye (CDBA) (−5.38 eV) > dye (AMCH) (−5.71 eV) > dye (CHMA) (−6.0 eV), it has been observed that the inclusion of so strongly activating groups like dimethylamine has the greatest impact on elevating the E_{HOMO} value for dye (CDBA) compared to dye (CHMA) and dye (AMCH). For the LUMO energies (E_{LUMO}) would have been in the following sequence of dye (CDBA) (−1.21 eV) > dye (CHMA) (−2.06 eV) and dye (AMCH) (−2.76 eV). As can be seen obviously, the decrease in the number of rings may lead to an increase in the energy of LUMO, although the following trend has been observed with energy gap values is dye (CDBA) (4.17 eV) > dye (CHMA) (3.94 eV) > dye (AMCH) (2.95 eV) (table 2). This decrease in the energy gap value of dye (AMCH) is probably due to the increasing extension of the π-conjugated system along the molecule. This revealed that improvement in the conjugated extension can efficiently minimize the energy gaps. The rise in the HOMO–LUMO gap enhances kinetic stability and minimizes chemical reactivity. The dyes with smaller energy gaps would be more effective for DSSCs.

The E_{HOMO} values for dye (CHMA) in all used solvents indicate slight increase of about (−0.05 eV), whereas a little decrease was observed in the E_{LUMO} values around (−0.05 eV) with DMF, CH_3CN and C_2H_5OH, while found to be (−0.06 eV) with DMSO than those values of the E_{HOMO} and E_{LUMO} in the gas phase, respectively. The finding results reveal that the solvents were not having the significant influence to elevate the E_{HOMO} and E_{LUMO} of CHMA.

For the dye (CDBA) the difference between E_{HOMO} values in the presence of solvents is increased by (−0.02 eV) with DMSO, CH_3CN and C_2H_5OH and around (−0.01 eV) for DMF, while the E_{LUMO} values were decreased by (−0.28 eV) in DMF and (−0.29 eV) in DMSO, CH_3CN and C_2H_5OH than those values in the gas phase, respectively.

Table 1. Geometry of dyes at B3LYP/6-31G(d) level of theory selected bond lengths.

Dye (CHMA)	Bond lengths (Å)	Dye (CDBA)	Bond lengths (Å)	Dye (AMCH)	Bond lengths (Å)
C7–N8	1.298	C10–N11	1.288	C7–N8	1.288
C7–H22	1.092	C10–H28	1.099	C7–H24	1.097
N8–N9	1.367	N11–N12	1.369	N8–N9	1.365
N9–H23	1.019	N12–H29	1.020	N9–H25	1.020
N9–C10	1.376	N12–C13	1.367	N9–C10	1.377
C10–O11	1.219	C13–O14	1.223	C10–O11	1.219
C10–C12	1.533	C13–C15	1.538	C10–C12	1.533
C12–H24	1.096	C15–H30	1.093	C12–H26	1.095
C12–H25	1.096	C15–H31	1.095	C12–H27	1.096
C12–C18	1.462	C15–C16	1.464	C12–C21	1.462
C18–N19	1.160	C16–N17	1.161	C21–N22	1.160

Table 2. HOMO energies (E_{HOMO}), LUMO energies (E_{LUMO}) and energy gaps (E_{gap}) in eV of dyes in the gas phase and different solvents at B3LYP/6-311G** level of theory.

Dyes	Gas phase	DMF	DMSO	CH_3CN	C_2H_5OH
E_{HOMO}					
CHMA	−6.00	−5.95	−5.95	−5.95	−5.96
CDBA	−5.38	−5.37	−5.36	−5.36	−5.36
AMCH	−5.71	−5.24	−5.48	−5.24	−5.25
E_{LUMO}					
CHMA	−2.06	−2.11	−2.10	−2.11	−2.11
CDBA	−1.22	−1.50	−1.51	−1.51	−1.51
AMCH	−2.77	−2.28	−2.53	−2.28	−2.28
E_{gap}					
CHMA	3.94	3.84	3.85	3.84	3.85
CDBA	4.16	3.87	3.85	3.85	3.85
AMCH	2.94	2.96	2.95	2.96	2.97

The results revealed that the solvents have no major influence to elevate the E_{HOMO} values.

The increase in the E_{HOMO} values for dye (AMCH) was found to be (−0.47 eV) with DMF and CH_3CN, (−0.46 eV) in C_2H_5OH and (−0.23 eV) in DMSO. But, the E_{LUMO} values are also higher (−0.24 eV) in the presence of DMSO and (−0.49 eV) in DMF, CH_3CN and C_2H_5OH than the E_{HOMO} and E_{LUMO} values in the gas phase, respectively. Therefore, we can say based on these findings the solvents have the significant influence to elevate the E_{HOMO} and E_{LUMO} values of AMCH.

The HOMO–LUMO energy gaps (E_{gap}) obtained for dye (CHMA) showed the decrease was 0.10 eV in DMF and CH_3CN, 0.09 eV in DMSO and C_2H_5OH. As for the dye (CDBA), the decrease was 0.29 eV in DMF and 0.31 eV in CH_3CN, DMSO and C_2H_5OH. But, the increase for the dye (AMCH) was 0.02 eV in DMF and CH_3CN, 0.01 eV in DMSO and 0.03 eV in C_2H_5OH compared to the values of

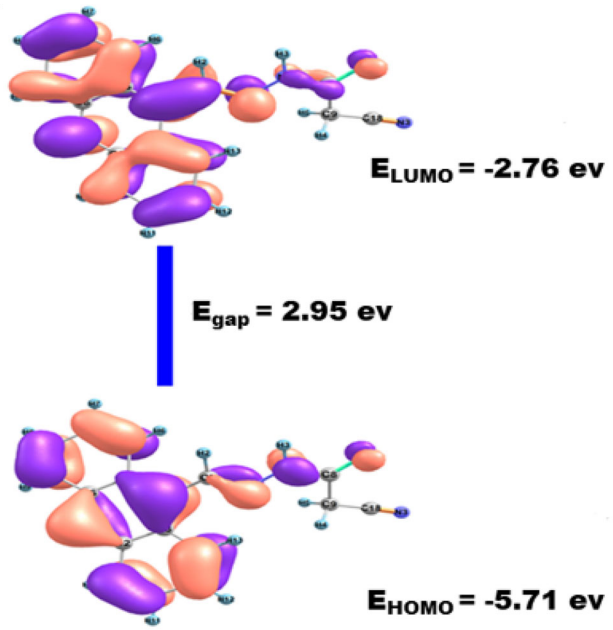

Figure 2. HOMO and LUMO presentation of dye (AMCH) in B3LYP/6-311G** level of theory.

the E_{gap} in the gas phase. The AMCH exhibited lowest energy gap due to the elevation of E_{HOMO} and E_{LUMO} values and will be red-shifted in all solvents as compared to CHMA and CDBA, respectively. Therefore, AMCH will be the best sensitizer in DSSCs. The HOMO and LUMO energy level, energy gap of all the prepared dyes obtained from DFT calculation and energy levels analogous to the valence and conduction band of TiO_2 [61,62] are plotted and shown in figure 3. In addition, the driving force of electron injection from dye to semiconductor also depends on the HOMO, LUMO and energy gap of dye. The potential prerequisite to flabbergast is implemented by the energy level offset of the LUMO of the excited and conduction band of TiO_2. Our computational studies revealed that

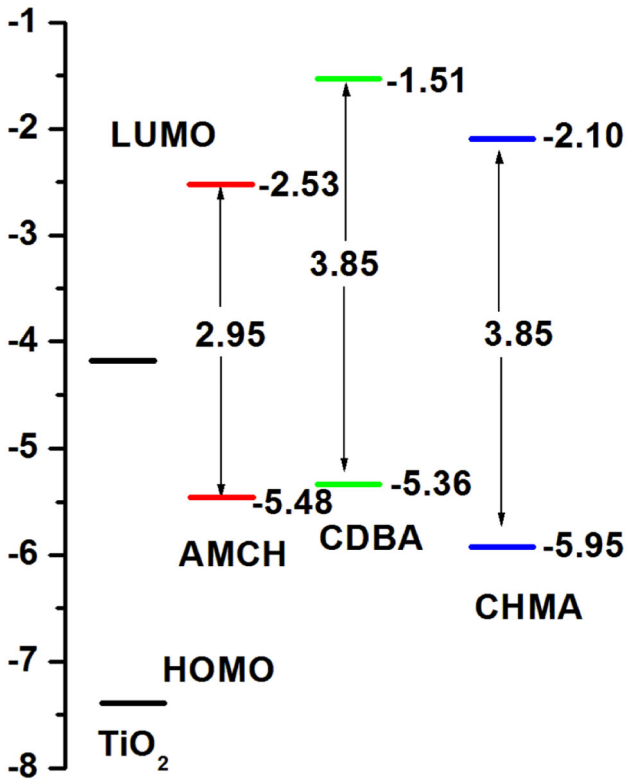

Figure 3. HOMO and LUMO energy level, energy gap of all prepared dyes obtained from DFT calculation and energy levels analogous to the valence and conduction band of TiO_2.

AMCH need very low energy as compared to CHMA and CDBA, respectively.

After working on a study on the effect of solvents on the computed absorption spectra of the synthesized dyes, the calculations were carried out in the gas phase (as a control), DMSO, DMF, ethanol and acetonitrile solvents using the TD-DFT/PCM method. The absorption peaks of dye (CHMA) to dye (AMCH) in a polar solvent have been observed and the bands ranged between 430 and 358 nm (supplementary figures S5–S7). The absorption spectra of the three dyes exhibit two bands; the first band was from 240 to 330 nm, while the second band was between 311 and 462 nm. With regards to the three dyes, it was found that alteration of the solvents did not have a considerable influence on the calculated absorption spectra towards redshift, while a little bit of change with DMSO solvent was experimentally observed, where the absorption peaks have shown behaviour towards redshift. On the other hand, the computed maximum absorption peaks of dye (AMCH) were shown a redshift, which may be due to the strong π-conjugated system.

Supplementary figures S8 and S9 exhibit the absorption peaks of dye (CHMA) to dye (AMCH) in benzene (nonpolar solvent) and acetonitrile (a polar solvent). With regard to the nonpolar solvent, it was found that the alteration of the solvents did not have a considerable influence on the calculated absorption spectra.

Supplementary figures S10–S13 represent the experimental UV–visible absorption spectra of dyes in diverse solvents. In general, the prepared dyes showed two absorption bands in the range of 250–500 nm. The absorption bands around 310–340 correspond to π–π* electron transition to conjugated molecule, whereas the wavelengths in the range of 376–472 nm are endorsed to the intramolecular charge transfer from donor to acceptor group that delivers effective charge separation in the excited state [63]. The alterations of solvents against all prepared dyes did not have any considerable effect in the absorption spectra towards redshift, but they showed slight red-shifted in DMSO. Dye (AMCH) exhibits a redshift absorption spectrum (435 nm) is relative to dye (CHMA) (386 nm) and dye (CDBA) (381 nm), which can be endorsed to the presence of the additional π-conjugated system in dye (AMCH). Therefore, dye (AMCH) shows low band gap between HOMO and LUMO and it pointed towards a more effective light-harvesting dye than the other two dyes [64]. It is clear from the figures that the direction of absorption spectra towards redshift of dye (CHMA), dye (CDBA) and dye (AMCH) in diverse solvents is acetonitrile < ethanol < DMF < DMSO. The comparative values of calculated and experimental results are presented in table 3.

3.3 *Reorganization energies*

We applied B3LYP/6-31G** level of theory to calculate the hole (λ^+) and electron (λ^-) reorganization energies of all prepared dyes and compared hole and electron reorganization energies values. It is used to assess the charge transfer rate and balance [65]. The results revealed that the calculated hole reorganization energies of all prepared dyes are smaller than electron reorganization energies values demonstrating that it might be well hole transfer material and *vice versa* [66]. We noted from figure 4 that the hole reorganization energy of dye (AMCH) is smaller than dye

Table 3. Experimental (Exp) absorption spectra and calculated (Calc) absorption spectra in B3LYP/6-311G** level of dye (CHMA), dye (CDBA) and dye (AMCH) in the gas phase and elected solvents.

Dyes	Gas phase	DMF	DMSO	CH_3CN	C_2H_5OH
λ_{max} (Calc)					
CHMA	338	358	358	357	357
CDBA	311	346	347	345	346
AMCH	452	427	462	455	456
λ_{max} (Exp)					
CHMA		383	386	379	381
CDBA		377	381	377	376
AMCH		400	405	425	472

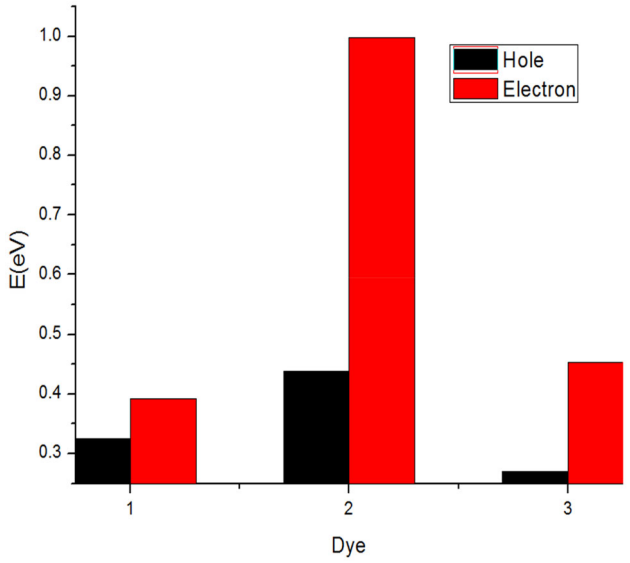

Figure 4. Hole and electron reorganization energies of dye-1 (CHMA), dye-2 (CDBA) and dye-3 (AMCH) in eV at the B3LYP/6-31G** level of theory.

CHMA and dye CDBA due to the presence of strong π-conjugated system, would be better hole transfer materials and show CT ability. Hole transporter means p-type and electron transporter means n-type. On the basis of HOMO, LUMO, IP, optical band gap and reorganization, it is suggested that all prepared dyes would be better charge transfer materials.

3.4 *Optical properties*

The energy band gap values help to extrapolate the performance of DSSCs. The minimal energy gap (E_g) of dyes detects the redshift in the wavelengths of the absorption spectra and minimizes the band gap of dyes leading to the electron excite faster from the HOMO into the LUMO and just requires lower energy to the recombination of the electrons and produces high fill factor (FF). Moreover, the band gaps are correlated to the range of absorbed wavelength, increasing the absorption wavelength and decreasing the band gap. The following equation is used to calculate the optical band gap (E_g):

$$(Ah\upsilon)^n = B\left(h\upsilon - E_g\right), \tag{1}$$

where $h\upsilon$ is the photon energy, A represents absorbance, B represents constant related to the material and n indicates either 2 or 1/2 for direct transition and indirect transition, respectively. Therefore, the optical band gap for the absorption peak is obtained by extending the linear portion of the $(Ah\upsilon)^n - h\upsilon$ curve to zero, as illustrated in supplementary figures S15–S17 and the values are mentioned in table 3.

The E_{gap} (Calc) values for the three dyes in different solvents range from 2.95 to 3.87 eV, while the E_{gap} (Exp) values range from 2.73 to 3.22 eV. It is clear from the table that the dye (AMCH) possesses minimal values of the energy gap with all solvents that were used. The reason behind the decrease in the energy gap values, observed in dye (AMCH), can be attributed to the conjugated chain length, where the increase in the chain length of the conjugated system leads to the decrease in the energy band gap. It is also clear from supplementary figures S18–S20 and table 4 that the energy gap values that have been evaluated computationally and experimentally are in good agreement with each other.

Table 4. Calculated energy gap E_{gap} (Calc), experimental energy gap E_{gap} (Exp) in different solvents.

Dyes	Gas phase	DMF	DMSO	CH_3CN	C_2H_5OH
E_{gap} (Calc)					
CHMA	3.94	3.84	3.85	3.84	3.85
CDBA	4.16	3.87	3.85	3.85	3.85
AMCH	2.94	2.96	2.95	2.96	2.97
E_{gap} (Exp)					
CHMA		3.14	3.13	3.16	3.15
CDBA		3.20	3.16	3.23	3.20
AMCH		2.76	2.75	2.79	2.78

3.5 *Photovoltaic performance*

The device structure consists of a working electrode of TiO_2 sensitized with the prepared organic dyes followed by the counter electrode of Pt. The current–voltage characteristics of DSSCs based on organic dyes for an area of 1 cm^2, under 100 mW cm^{-2} illumination powers are shown in figure 5. A list of output parameters with standard dye and various organic dyes is given in table 5.

The dye (CHMA) cell gave a short-circuit photocurrent density (J_{sc}) of 4.9 mA cm^{-2}, an open-circuit voltage (V_{oc}) of 0.60 V and a FF of 0.64% with the illumination power (P_{in}) 100 mW cm^{-2}, corresponding to an overall conversion efficiency of 1.92%. The dye (CDBA) gave J_{sc} of 3.6 mA cm^{-2}, V_{oc} of 0.55 V and FF of 0.68% leading PCE 1.34%. The PCE of dye (AMCH) has been observed (2.61) with J_{sc} of 6.7 mA cm^{-2}, V_{oc} of 0.60 V and FF of 0.63% the standard dye (N719) results in a J_{sc} of 12 mA cm^{-2}, V_{oc} of 0.70 V and FF of 0.72% with an efficiency of 6.1%. The highest efficiency in the case of the dye (AMCH) sensitizer is probably due to the presence of the strong π-conjugated system. Moreover, the redshift of the absorption wavelength reduces the energy gap and ionization potential, the hole/electron's ability of dye (AMCH) is enhanced as compared to the other two dyes. The solar energy to electricity conversion efficiency of the present organic dyes could be enriched by extending the conjugated length of organic dyes or integrating more cyano or carboxylic or cyano and carboxylic group. The syntheses of high-efficiency

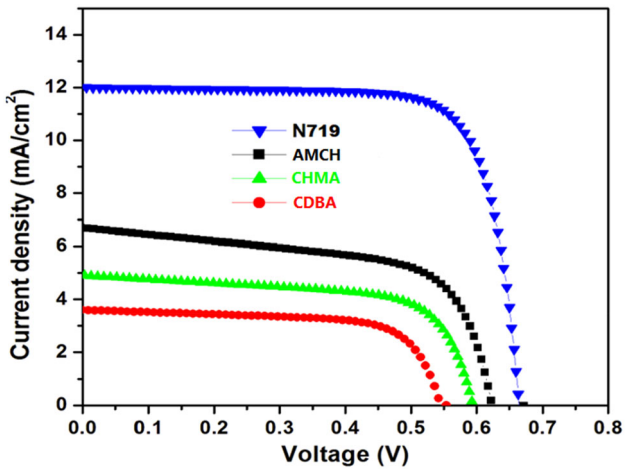

Figure 5. Current–voltage characteristics of DSSCs based on (**a**) dye (CHMA), (**b**) dye (CDBA), (**c**) dye (AMCH) and (**d**) N719 commercial dye (area: 1 cm^2).

Table 5. Photovoltaic performance of DSSCs based on dyes.

Dye	V_{oc} (V)	J_{sc} (mA cm^{-2})	Fill factor (FF)	Efficiency η (%)
CHMA	0.609	4.9	0.6440	1.92
CDBA	0.55	3.6	0.6811	1.34
AMCH	0.609	6.7	0.6398	2.61
N719	0.70	12	0.72	6.1

organic dyes are still in progress in our laboratory. Furthermore, the larger (V_{oc}) of dye (AMCH) is endorsed to the suppressed charge recombination at the nanocrystalline/dye/redox electrolyte interface [67]. The lower photocurrent efficiency of dye (CHMA) and dye (CDBA)-sensitized devices is attributed to the blue-shifted dyes with a higher energy band-gap than that of the dye (AMCH) dye. Previously [68], in our laboratory we have used different organic dyes (2-{4-[2-(2-hydroxybenzylidene)hydrazino]phenyl}ethylene-1,1,2-tricarbonitrile (D-1) and 2-{4-[2-(4-hydroxybenzylidene)hydrazino]phenyl}ethylene-1,1,2-tricarbonitrile (D-2)) and constructed as hetero-junction solar cell materials by organic–inorganic heterojunction (dye/Si/TiO_2), the efficiency was estimated by using the distinct incident power 30, 50 and 70 mW cm^{-2} and the obtained maximum efficiency up to 3.6% for D-2. The effect of the presence of the electron-donating group at the *para* position and red-shifted absorption wavelengths with respect to D-1 on efficiency was observed.

4. Conclusions

This study summarized the synthesis and characterization of three hydrazone-based sensitizers (dye CHMA, dye CDBA and dye AMCH) by means of various analytical techniques such as FT-IR, UV–visible, ^{1}H NMR and ^{13}C NMR to find out the most possible selection for DSSCs. The absorption spectra of dye AMCH are red-shifted as compared to dye CHMA and dye CDBA, perhaps due to extended π-conjugation length. The small HOMO–LUMO energy gap revealed these dyes would be better sensitizers for DSSCs, which are in good agreement with the values obtained experimentally. We used fabricated device to measure *J–V* characteristics and the results show the higher efficiency (2.61) in the case of the dye AMCH sensitizer is probably due to the presence of the strong π-conjugated system. Moreover, red-shift of the absorption wavelength reduces the energy gap and ionization potential, the hole/electron ability of dye AMCH is enhanced as compared to other two dyes. The solar energy to electricity conversion efficiency of the present organic dyes could be enriched by extending the conjugated length of organic dyes or integrating more cyano or carboxylic or cyano and carboxylic group. The syntheses of high-efficiency organic dyes are still in progress in our laboratory.

Acknowledgement

We thank King Abdul Aziz City of Science and Technology (KACST) for their financial support to Shuhrah Ali S Allami with Grant Number 1-17-01-010-0018.

References

[1] Potocnik J 2007 *Science* **315** 810
[2] Oregan B and Grätzel M 1991 *Nature* **353** 737
[3] Wu Y, Zhu W-H, Zakeeruddin S M and Grätzel M 2015 *ACS Appl. Mater. Interfaces* **7** 9307
[4] Ye M, Wen X, Wang M, Iocozzia J, Zhang N, Lin C *et al* 2015 *Mater. Today* **18** 155
[5] Wu M and Ma T 2014 *J. Phys. Chem. C* **118** 16727
[6] Gong J, Sumathy K, Qiao Q and Zhou Z 2017 *Renew. Sust. Energ. Rev.* **68** 234
[7] Hagfeldt A, Boschloo G, Sun L, Kloo L and Pettersson H 2010 *Chem. Rev.* **110** 6595
[8] Ji Z, Natu G and Wu Y 2013 *ACS Appl. Mater. Interfaces* **5** 8641
[9] Ngo K T, Lee N A, Pinnace S D and Rochford J 2017 *Chem. Eur. J.* **23** 7621
[10] Liang M and Chen J 2013 *Chem. Soc. Rev.* **42** 3453
[11] Urbani M, Grätzel M, Nazeeruddin M K and Torres T 2014 *Chem. Rev.* **114** 12330
[12] Giribabu L and Kanaparthi R K 2013 *Curr. Sci.* **104** 847
[13] Wang C L, Lan C M, Hong S H, Wang Y F, Pan T Y, Chang C W *et al* 2012 *Energy Environ. Sci.* **5** 6933
[14] Green M A 2001 *Prog. Photovoltics* **9** 123
[15] Calogero G, Bartolotta A, Marco G D, Carlo A D and Bonaccorso F 2015 *Chem. Soc. Rev.* **44** 3244
[16] Yao Z, Zhang M, Wu H, Yang L, Li R and Wang P 2015 *J. Am. Chem. Soc.* **137** 3799

[17] Calogero G, Yum J-H, Sinopoli A, Marco G D, Grätzel M and Nazeeruddin M K 2012 *Sol. Energy* **86** 1563
[18] Calogero G, Sinopoli A, Citro I, Marco G D, Petrov V, Diniz A M *et al* 2013 *Photochem. Photobiol. Sci.* **12** 883
[19] Koumura N, Wang Z-S, Mori S, Miyashita M, Suzuki E and Hara K 2006 *J. Am. Chem. Soc.* **128** 14256
[20] Mishra A, Fischer M K R and Bäuerle P 2009 *Angew. Chem.* **48** 2474
[21] Feldt S M, Gibson E A, Gabrielsson E, Sun L, Boschloo G and Hagfeldt A 2010 *J. Am. Chem. Soc.* **132** 16714
[22] Yella A, Lee H-W, Tsao H N, Yi C, Chandiran A K, Nazeeruddin M K *et al* 2011 *Science* **334** 629
[23] Gómez-Ortíz N, Vázquez-Maldonado I, Pérez-Espadas A, Mena-Rejón G, Azamar-Barrios J and Oskam G 2010 *Sol. Energy Mater. Sol. Cells* **94** 40
[24] Wongcharee K, Meeyoo V and Chavadej S 2007 *Sol. Energy Mater. Sol. Cells* **91** 566
[25] Li S-L, Jiang K-J, Shao K-F and Yang L-M 2006 *Chem. Commun.* 2792
[26] Hara K, Sato T, Katoh R, Furube A, Yoshihara T, Murai M *et al* 2005 *Adv. Funct. Mater.* **15** 246
[27] Lygaitis R, Getautis V and Grazulevicius J V 2008 *Chem. Soc. Rev.* **37** 770
[28] Kim S and Yoon J-Y 2004 *Sci. Synth.* **27** 671
[29] Uribe-Romo F J, Doonan C J, Furukawa H, Oisaki K and Yaghi O M 2011 *J. Am. Chem. Soc.* **133** 11478
[30] Ulrich S and Dumy P 2014 *Chem. Commun.* **50** 5810
[31] Raue R, Brack A and Lange K H 1991 *Angew. Chem.* **30** 1643
[32] Laurinaviciute R, Mimaite V, Ostrauskaite J, Grazulevicius J V and Jankauskas V 2014 *Synth. Met.* **197** 1
[33] Michaleviciute A, Buika G, Grazulevicius J V, Tran-Van F, Chevrot C and Jankauskas V 2007 *Mol. Cryst. Liq. Cryst.* **468** 107
[34] Shen P, Liu X, Jiang S, Huang Y, Yi L, Zhao B *et al* 2011 *Org. Electron.* **12** 1992
[35] Shen P, Liu X, Jiang S, Wang L, Yi L, Ye D *et al* 2012 *Dyes Pigm.* **92** 1042
[36] Aich R, Tran-Van F, Goubard F, Beouch L, Michaleviciute A, Grazulevicius J *et al* 2008 *Thin Solid Films* **516** 7260
[37] Li L-L and Diau E W-G 2013 *Chem. Soc. Rev.* **42** 291
[38] Birel Ö, Nadeem S and Duman H 2017 *J. Fluoresc.* **27** 1075
[39] Ladomenou K, Kitsopoulos T N, Sharma G D and Coutsolelos A G 2014 *RSC Adv.* **4** 21379
[40] Salzner U, Lagowski J B, Pickup P G and Poirier R A 1998 *Synth. Met.* **96** 177
[41] Koch W, Holthausen M C and Kaupp M 2001 *Angew. Chem.* **113** 989
[42] Irfan A and Al-Sehemi A G 2012 *J. Chem. Soc. Pak.* **34** 350
[43] Nazeeruddin M K, De Angelis F, Fantacci S, Selloni A, Viscardi G, Liska P *et al* 2005 *J. Am. Chem. Soc.* **127** 16835
[44] Liu Z 2008 *J. Mol. Struct. Theochem.* **862** 44
[45] Sánchez-Carrera R S, Coropceanu V, da Silva Filho D A, Friedlein R, Osikowicz W, Murdey R *et al* 2006 *J. Phys. Chem. B* **110** 18904
[46] Abbas G, Irfan A, Mir M and Khan A F 2013 *J. Mol. Struct.* **1050** 10
[47] Irfan A, Al-Sehemi A G, Muhammad S, Chaudhry A R, Al-Assiri M S, Jin R *et al* 2015 *C. R. Chim.* **18** 1289
[48] Al-Sehemi A G, Irfan A and Assiri A M 2012 *Theor. Chem. Acc.* **131** 1199
[49] Becke A D 1993 *J. Chem. Phys.* **98** 5648
[50] Lee C, Yang W and Parr R G 1988 *Phys. Rev. B: Condens. Matter* **37** 785
[51] Stephens P J, Devlin F J, Chabalowski C F and Frisch M J 1994 *J. Phys. Chem.* **98** 11623
[52] Lynch B J, Fast P L, Harris M and Truhlar D G 2000 *J. Phys. Chem. A* **104** 4811
[53] Perdew J P, Chevary J A, Vosko S H, Jackson K A, Pederson M R, Singh D J *et al* 1992 *Phys. Rev. B: Condens. Matter* **46** 6671
[54] Walsh P J, Gordon K C, Officer D L and Campbell W M 2006 *J. Mol. Struct. Theochem.* **759** 17
[55] Cleland D M, Gordon K C, Officer D L, Wagner P and Walsh P J 2009 *Spectrochim. Acta Part A* **74** 931
[56] Zhang C R, Liang W Z, Chen H S, Chen Y H, Wei Z Q and Wu Y Z 2008 *J. Mol. Struct. Theochem.* **862** 98
[57] Sun J, Song J, Zhao Y and Liang W Z 2007 *J. Chem. Phys.* **127** 234107
[58] Matthews D, Infelta P and Grätzel M 1996 *Sol. Energy Mater. Sol. Cells* **44** 119
[59] Al-Sehemi A G, Irfan A and Assiri M A 2014 *Chin. Chem. Lett.* **25** 609
[60] Frisch M J, Trucks G W, Schlegel H B, Scuseria G E, Robb M A, Cheeseman J R *et al* 2009 Gaussian 09 revision D.01, Wallingford, CT: Gaussian, Inc.
[61] Prima E C, Hidayat N N, Yuliarto B and Dipojono H K 2017 *Spectrochim. Acta Part A* **171** 112
[62] Ekanayake P, Kooh M R, Kumara N T, Lim A, Petra M I, Voo N Y *et al* 2013 *Chem. Phys. Lett.* **585** 121
[63] Liang M, Xu W, Cai F, Chen P, Peng B, Chen J *et al* 2007 *J. Phys. Chem. C* **111** 4465
[64] Guo M, Diao P, Ren Y-J, Meng F, Tian H and Cai S-M 2005 *Sol. Energy Mater. Sol. Cells* **88** 23
[65] Han D, Zhang G, Chai H, Zhang X and Zhao L 2013 *J. Lumin.* **138** 223
[66] Irfan A, Al-Sehemi A G and Al-Assiri M S 2013 *J. Mol. Graph. Model* **44** 168
[67] Palomares E, Clifford J N, Haque S A, Lutz T and Durrant J R 2003 *J. Am. Chem. Soc.* **125** 475
[68] Al-Sehemi A G, Irfan A, Al-Melfi M A M, Al-Ghamdi A A and Shalaan E 2014 *J. Photochem. Photobiol. A* **292** 1